Characteristic outflows with optimal transverse terms: the edges and corners coupling algorithm

By G. Lodato AND H. Pitsch

1. Motivation and objectives

The accuracy of compressible solvers is known to be, in general, strongly sensitive to the boundary solution. The flow properties at the boundaries are obtained by combining (a) numerical boundary conditions pertaining the information coming from the inside of the computational domain, and (b) physical boundary conditions obtained from some approximations of the outside flow features (Hirsch 1990). Based on the above classification, the overall performances of the boundary conditions in terms, in particular, of numerical reflection is affected, for the most part, by what is prescribed by the physical conditions and how the information is combined with their numerical counterpart.

Several different techniques have been proposed to deal with the mathematical formulation of the boundary problem, and the definition of open frontiers for the most general set of flow conditions is particularly challenging (see Givoli 2004; Colonius 2004; Nicoud 1999 and references cited therein for a review). The present study focuses on the class of characteristic boundary conditions which are obtained by reformulating the system of conservation laws in terms of the characteristic waves traveling in a fixed direction (generally, the normal to the boundary is chosen, even though different directions may be used as proposed by Bayliss & Turkel 1982; Roe 1989). Once a distinction is made between waves that leave and enter the computational domain, the boundary problem can be formulated as a set of numerical and physical boundary conditions to be imposed on outgoing and incoming waves, respectively.

The identification of incoming waves allows some level of control over boundary reflection, as the boundary condition can be designed to minimize incoming perturbations or to damp their amplitude while allowing smooth transients (Hedstrom 1979; Thompson 1987, 1990; Rudy & Strikwerda 1980). This technique was extended to the Navier-Stokes equations by Poinsot & Lele (1992) by providing the additional boundary conditions necessary for the viscous terms. This procedure is commonly referred to as Navier-Stokes Characteristic Boundary Conditions (NSCBC) and makes explicit use of the hypothesis that the flow field at the boundary may be approximated as inviscid and one-dimensional.

In order to overcome one of the main weaknesses of the NSCBC approach, i.e., the one-dimensional hypothesis, which may lead to significant numerical reflection for strongly three-dimensional flow fields, a series of modifications was discussed by different authors. Addressing directly the role played by the transverse convective and viscous terms, as well as the source terms in the case of reactive flows, Yoo *et al.* (2005) and Yoo & Im (2007) showed that an appropriate treatment of these terms in the computation of incoming waves improves the accuracy and convergence rate toward target values for selected relaxed quantities while reducing flow distortion. Following the above idea, in the specific context of structured codes on cartesian grids, a systematic procedure to solve transverse terms-induced wave coupling at the edges and corners of the computational domain was proposed by Lodato *et al.* (2008), leading to the 3D-NSCBC formulation.

A thorough analysis of the subsonic characteristic outflow boundary condition with transverse terms has been recently carried out by Lodato *et al.* (2010, 2011). By properly identifying the different contributions to the transverse terms in the characteristic equations, namely the transverse terms relevant to the material derivatives along the bi-characteristics and the coupling terms between the characteristic equations, a unifying formulation involving three relaxation parameters was presented. Resorting to the normal mode analysis, a parametric analysis of well-posedness was performed in order to establish the admissible bounds of the relaxation coefficients. Furthermore, inspection of the relevant matrix of reflection demonstrated that an optimal formulation—similar to the second-order subsonic outflow condition developed by Giles (1990)—that minimizes coupling between outgoing vorticity modes and incoming acoustic modes can be obtained.

Numerical tests on the inviscid convected vortex test case over different computational grids, for different base flow directions and at different Mach numbers, demonstrated that by using the above-mentioned optimal formulation, the boundary-induced numerical errors can be maintained relatively constant, regardless of the base flow direction with respect to the boundary plane. Comparable errors were also measured even when the computational mesh was characterized by a curved boundary, thus suggesting that even if boundary numerical perturbations cannot be completely removed due to the intrinsic limitations of the characteristic boundary conditions approach, the optimal formulation can be used to keep the errors under control even when the character of the flow at the boundary is difficult or impossible to be anticipated. The edges and corners coupling procedure for cartesian meshes proposed by Lodato *et al.* (2008) is here extended to this optimal formulation.

2. The NSCBC approach

Let us consider the local formulation of the Euler equations involving the vector of conservative variables $\widetilde{\boldsymbol{U}}$ and the flux vector in the kth direction $\widetilde{\boldsymbol{F}}^k$. Using Einstein summation convention for repeated indices, these may be written as

$$\frac{\partial \widetilde{\boldsymbol{U}}}{\partial t} + \frac{\partial \widetilde{\boldsymbol{F}}^k}{\partial x_k} = \boldsymbol{0}, \tag{2.1}$$

with

$$\widetilde{\boldsymbol{U}} = \begin{pmatrix} \rho \\ \rho u_1 \\ \rho u_2 \\ \rho u_3 \\ \rho e \end{pmatrix}, \quad \widetilde{\boldsymbol{F}}^k = \begin{pmatrix} \rho u_k \\ \rho u_1 u_k + \delta_{1k} p \\ \rho u_2 u_k + \delta_{2k} p \\ \rho u_3 u_k + \delta_{3k} p \\ (\rho e + p) u_k \end{pmatrix}. \tag{2.2}$$

In the above equations, ρ represents the fluid density, u_k is the velocity component in the kth direction, p is the pressure, δ_{ik} is the Kronecker's delta and e is the total energy, defined by the following relation:

$$\rho e = \frac{1}{2}\rho u_k u_k + \frac{p}{\gamma - 1}. \tag{2.3}$$

Introducing the Jacobians $\partial \widetilde{\boldsymbol{F}}^k / \partial \widetilde{\boldsymbol{U}}$ and the transformation matrix $\boldsymbol{P} = \partial \widetilde{\boldsymbol{U}} / \partial \boldsymbol{U}$ between primitive variables $\boldsymbol{U}$ and conservative variables $\widetilde{\boldsymbol{U}}$, Eq. (2.1) may be reduced in

quasi-linear form as (Hirsch 1990; Thompson 1987, 1990; Warming *et al.* 1975):

$$\frac{\partial \boldsymbol{U}}{\partial t} + \boldsymbol{A}^k \frac{\partial \boldsymbol{U}}{\partial x_k} = \boldsymbol{0}. \tag{2.4}$$

In particular, if the density, the three components of velocity and the pressure are chosen as primitive variables, the Jacobians $\boldsymbol{P}$ and $\boldsymbol{A}^k$ become

$$\boldsymbol{P} = \begin{pmatrix} 1 & 0 & 0 & 0 & 0 \\ u_1 & \rho & 0 & 0 & 0 \\ u_2 & 0 & \rho & 0 & 0 \\ u_3 & 0 & 0 & \rho & 0 \\ \frac{1}{2}u_k u_k & \rho u_1 & \rho u_2 & \rho u_3 & 1/\varkappa \end{pmatrix}, \tag{2.5}$$

$$\boldsymbol{P}^{-1} = \begin{pmatrix} 1 & 0 & 0 & 0 & 0 \\ -u_1/\rho & 1/\rho & 0 & 0 & 0 \\ -u_2/\rho & 0 & 1/\rho & 0 & 0 \\ -u_3/\rho & 0 & 0 & 1/\rho & 0 \\ \frac{1}{2}u_k u_k \varkappa & -\varkappa u_1 & -\varkappa u_2 & -\varkappa u_3 & \varkappa \end{pmatrix}, \tag{2.6}$$

where $\varkappa = \gamma - 1$, and

$$\boldsymbol{A}^k = \begin{pmatrix} u_k & \delta_{1k}\rho & \delta_{2k}\rho & \delta_{3k}\rho & 0 \\ 0 & u_k & 0 & 0 & \delta_{1k}/\rho \\ 0 & 0 & u_k & 0 & \delta_{2k}/\rho \\ 0 & 0 & 0 & u_k & \delta_{3k}/\rho \\ 0 & \delta_{1k}\rho a^2 & \delta_{2k}\rho a^2 & \delta_{3k}\rho a^2 & u_k \end{pmatrix}, \tag{2.7}$$

where $a = \sqrt{\gamma p/\rho}$ is the speed of sound.

In order to build characteristic boundary conditions, Eq. (2.4) is first rewritten into a form that makes explicit the characteristic signals propagating along a specified direction, e.g. normal to the boundary. Physical boundary conditions are then imposed on characteristic waves coming from the outside of the domain, based on some information about the exterior domain (Thompson 1987, 1990; Poinsot & Lele 1992; Yoo & Im 2007; Lodato *et al.* 2008). In order to do so, considering for simplicity a plane boundary ortogonal to the x_1 direction, the $\boldsymbol{A}^1$ matrix is first diagonalized using the following transformation:

$$\boldsymbol{\Lambda} = \boldsymbol{S}_1^{-1} \boldsymbol{A}^1 \boldsymbol{S}_1, \tag{2.8}$$

where $\boldsymbol{\Lambda} = \mathrm{diag}(u_1 - a, u_1, u_1, u_1, u_1 + a)$ and $\boldsymbol{S}_1^{-1}$ and $\boldsymbol{S}_1$ are the relevant transformation matrices built with the left and right eigenvectors of $\boldsymbol{A}^1$:

$$\boldsymbol{S}_1 = \begin{pmatrix} 1/(2a^2) & 1/a^2 & 0 & 0 & 1/(2a^2) \\ -1/(2\rho a) & 0 & 0 & 0 & 1/(2\rho a) \\ 0 & 0 & 1 & 0 & 0 \\ 0 & 0 & 0 & 1 & 0 \\ 1/2 & 0 & 0 & 0 & 1/2 \end{pmatrix}, \tag{2.9}$$

$$\boldsymbol{S}_1^{-1} = \begin{pmatrix} 0 & -\rho a & 0 & 0 & 1 \\ a^2 & 0 & 0 & 0 & -1 \\ 0 & 0 & 1 & 0 & 0 \\ 0 & 0 & 0 & 1 & 0 \\ 0 & \rho a & 0 & 0 & 1 \end{pmatrix}. \tag{2.10}$$

Hence, the characteristic waves may be made explicit by combining Eqs. (2.4) and (2.8)

as

$$\frac{\partial \boldsymbol{U}}{\partial t} + \boldsymbol{S}_1 \boldsymbol{\mathcal{L}} + \boldsymbol{A}^t \frac{\partial \boldsymbol{U}}{\partial x_t} = \boldsymbol{0}, \tag{2.11}$$

where we have introduced the wave amplitude variations $\boldsymbol{\mathcal{L}} = \boldsymbol{\Lambda}\boldsymbol{S}_1^{-1}\partial \boldsymbol{U}/\partial x_1$ and the repeated t index means summation over the transverse directions x_2 and x_3.

The vector $\boldsymbol{\mathcal{L}}$ is a function of the gradient of the solution along x_1 only; furthermore, each wave $\mathcal{L}_i$ is characterized by a certain propagation velocity λ_i, i.e.the corresponding diagonal component of the matrix $\boldsymbol{\Lambda}$. For a subsonic flow, three of these waves travel with the local velocity u_1, namely the entropy and the two shear waves (in the present case, $\mathcal{L}_2$, $\mathcal{L}_3$ and $\mathcal{L}_4$, respectively), whereas the two acoustic signals are always left- and right-going ($\mathcal{L}_1$ and $\mathcal{L}_5$, respectively). If we focus our attention to an outflow boundary on the right of the domain, i.e. $u_1 \geq 0$ and $x_1 = L$, there is one incoming wave $\mathcal{L}_1$ and four outgoing waves. The boundary condition problem is reduced to the determination of the incoming one from some knowledge about the exterior domain.

Assuming, for instance, that the flow is one-dimensional at the boundary, Eq. (2.11) may be simplified as

$$\boldsymbol{S}_1^{-1} \frac{\partial \boldsymbol{U}}{\partial t} + \boldsymbol{\mathcal{L}} = \boldsymbol{0}, \tag{2.12}$$

which may be used to derive useful relations between outgoing and incoming waves and the time derivative of the primitive variables (Thompson 1987, 1990; Poinsot & Lele 1992). Using Eq. (2.12) and the results from Rudy & Strikwerda (1980), Poinsot & Lele (1992) derived the subsonic outflow boundary condition

$$\mathcal{L}_1 = \sigma \frac{a(1 - Ma^2)}{L}(p - p_\infty), \tag{2.13}$$

where σ is a relaxation coefficient, Ma is a typical Mach number for the flow field under study, L is a reference length and p_∞ is the reference outflow pressure. The Thompson's non-reflecting outflow condition may be recovered from the above relation by setting $\sigma = 0$.

If transverse effects are not negligible, Eq. (2.12) becomes too stringent to correctly reproduce the flow field at the boundary without numerical reflection; hence, a more general formulation may be obtained based on the use of Eq. (2.11), as proposed by Yoo *et al.* (2005); Yoo & Im (2007). Eq. (2.11) is rewritten as

$$\boldsymbol{S}_1^{-1} \frac{\partial \boldsymbol{U}}{\partial t} + \boldsymbol{\mathcal{L}} = \boldsymbol{T}, \tag{2.14}$$

where $\boldsymbol{T} = -\boldsymbol{S}_1^{-1}\boldsymbol{A}^t \partial \boldsymbol{U}/\partial x_t$ $(t = 2, 3)$. Using again the condition proposed by Rudy & Strikwerda (1980), the boundary condition for $\mathcal{L}_1$ then becomes

$$\mathcal{L}_1 = \sigma \frac{a(1 - Ma^2)}{L}(p - p_\infty) + (1 - \beta_t)T_1 + \beta_t T_1^{\mathrm{ex}}, \tag{2.15}$$

where β_t is a transverse relaxation coefficient and T_1^{ex} is a known estimation of the transverse term T_1 toward which this last is relaxed.

Eq. (2.15) is quite effective in preventing significant reflection at low Mach number, giving interesting results in the classical inviscid vortex convection test case, as well as in other more complex flows (Yoo *et al.* 2005; Yoo & Im 2007; Lodato *et al.* 2008). Nonetheless, as pointed out by Lodato *et al.* (2008), when the Mach number is increased, Eq. (2.15) becomes less and less effective, and stronger perturbations are observed at the outflow.

3. Optimal inclusion of transverse terms

In a recent work by Lodato *et al.* (2010), the role played by different transverse terms in the characteristic equations was carefully analyzed in the most general case of non-orthogonal reference frames. The main idea was to make a distinction between the transverse terms relevant to the material derivatives along the bi-characteristics and the coupling terms between the characteristic equations. Grounded on this fundamental distinction between different contributions to the transverse terms, it was demonstrated by normal mode analysis (Kreiss 1970) that there exists an optimal way to include the transverse terms in the formulation of the subsonic non-reflecting outflow condition such that coupling between outgoing vorticity waves and incoming acoustic waves can be minimized, thus allowing a significant reduction of numerical reflection, especially when the base flow is not orthogonal to the boundary. The idea behind the above-mentioned classification of transverse effects is briefly summarized below for the simplest case of an orthogonal reference frame, which is particularly relevant for the generalization of the edges and coupling algorithm for cartesian grids that will be detailed in the next section.

Premultiplying Eq. (2.4) by $\boldsymbol{S}_1^{-1}$ we get

$$\frac{\partial \boldsymbol{W}}{\partial t} + \boldsymbol{\mathcal{L}} + \boldsymbol{\mathcal{L}}_t - \overline{\boldsymbol{T}} = \boldsymbol{0}, \tag{3.1}$$

where

$$\delta \boldsymbol{W} = \boldsymbol{S}_1^{-1} \delta \boldsymbol{U} = \begin{pmatrix} \delta p - \rho a \delta u_1 \\ a^2 \delta \rho - \delta p \\ \delta u_2 \\ \delta u_3 \\ \delta p + \rho a \delta u_1 \end{pmatrix} \tag{3.2}$$

represents a small increment of the characteristic variables $\boldsymbol{W}$ and $\boldsymbol{\mathcal{L}}$ is defined as before, i.e.

$$\boldsymbol{\mathcal{L}} = \boldsymbol{S}_1^{-1} \boldsymbol{A}^1 \frac{\partial \boldsymbol{U}}{\partial x_1} = \begin{pmatrix} (u_1 - a)\left(\frac{\partial p}{\partial x_1} - \rho a \frac{\partial u_1}{\partial x_1}\right) \\ u_1 \left(a^2 \frac{\partial \rho}{\partial x_1} - \frac{\partial p}{\partial x_1}\right) \\ u_1 \frac{\partial u_2}{\partial x_1} \\ u_1 \frac{\partial u_3}{\partial x_1} \\ (u_1 + a)\left(\frac{\partial p}{\partial x_1} + \rho a \frac{\partial u_1}{\partial x_1}\right) \end{pmatrix} = \boldsymbol{\Lambda} \frac{\partial \boldsymbol{W}}{\partial x_1}. \tag{3.3}$$

The other two terms are defined as

$$\boldsymbol{\mathcal{L}}_t = \begin{pmatrix} u_t \left(\frac{\partial p}{\partial x_t} - \rho a \frac{\partial u_1}{\partial x_t}\right) \\ u_t \left(a^2 \frac{\partial \rho}{\partial x_t} - \frac{\partial p}{\partial x_t}\right) \\ u_t \frac{\partial u_2}{\partial x_t} \\ u_t \frac{\partial u_3}{\partial x_t} \\ u_t \left(\frac{\partial p}{\partial x_t} + \rho a \frac{\partial u_1}{\partial x_t}\right) \end{pmatrix} = u_t \frac{\partial \boldsymbol{W}}{\partial x_t}, \quad \overline{\boldsymbol{T}} = \begin{pmatrix} -\rho a^2 \frac{\partial u_t}{\partial x_t} \\ 0 \\ -\frac{1}{\rho} \frac{\partial p}{\partial x_2} \\ -\frac{1}{\rho} \frac{\partial p}{\partial x_3} \\ -\rho a^2 \frac{\partial u_t}{\partial x_t} \end{pmatrix}, \tag{3.4}$$

where the repeated index t stands for summation over the transverse components 2 and 3. The advantage of the above reformulation is that if we now introduce the material derivative along the bi-characteristic $(\boldsymbol{u} \pm a\boldsymbol{n})$ (Hirsch 1990)

$$\frac{\mathrm{d}_\mathrm{b}^\pm}{\mathrm{d}t} = \frac{\partial}{\partial t} + (u_j \pm a n_j) \frac{\partial}{\partial x_j}, \tag{3.5}$$

and the *usual* material derivative $\mathrm{d}/\mathrm{d}t$ along a streamline, Eq. (3.1) can be rearranged as

$$\begin{cases} \dfrac{\mathrm{d}_\mathrm{b}^- W_1}{\mathrm{d}t} = \overline{T}_1 = -\rho a^2 \dfrac{\partial u_t}{\partial x_t}, \\ \dfrac{\mathrm{d}W_2}{\mathrm{d}t} = \overline{T}_2 = 0, \\ \dfrac{\mathrm{d}W_3}{\mathrm{d}t} = \overline{T}_3 = -\dfrac{1}{\rho}\dfrac{\partial p}{\partial x_2}, \\ \dfrac{\mathrm{d}W_4}{\mathrm{d}t} = \overline{T}_4 = -\dfrac{1}{\rho}\dfrac{\partial p}{\partial x_3}, \\ \dfrac{\mathrm{d}_\mathrm{b}^+ W_5}{\mathrm{d}t} = \overline{T}_5 = -\rho a^2 \dfrac{\partial u_t}{\partial x_t}, \end{cases} \tag{3.6}$$

where all the transverse effects connected with the material derivatives are grouped inside the vector $\boldsymbol{\mathcal{L}}_t$, whereas the vector $\overline{\boldsymbol{T}}$ represents the coupling term between the characteristic equations.

Given the profoundly different nature of the transverse terms represented by $\boldsymbol{\mathcal{L}}_t$ and $\overline{\boldsymbol{T}}$, it is argued that different amounts of relaxation may be needed when defining characteristic boundary condition with *transverse relaxation*. Therefore, starting from Eq. (2.15) and supposing for simplicity that T_1^{ex} is identically zero, such a distinction is readily obtained by splitting T_1 as $\overline{T}_1 - \mathcal{L}_{t1}$ and by using different relaxation coefficients. The boundary condition for $\mathcal{L}_1$ then becomes

$$\mathcal{L}_1 = K(p - p_\infty) - (1 - \beta_l)\mathcal{L}_{t1} + (1 - \beta_t)\overline{T}_1, \tag{3.7}$$

where we have set $K = \sigma a(1 - Ma^2)/L$ and we have defined β_l as the relaxation coefficient for $\mathcal{L}_{t1}$.

In the work by Lodato *et al.* (2010, 2011), the analysis of well-posedness and reflection, and a series of numerical tests on the convected vortex at different angles and different Mach numbers led to the conclusion that, in order to minimize the coupling between outgoing vorticity modes and incoming acoustic modes, the relaxation coefficient β_l should be set equal to 1, thus leading to the following optimal definition of the incoming wave for the subsonic outflow boundary condition

$$\mathcal{L}_1 = K(p - p_\infty) + (1 - \beta_t)\overline{T}_1. \tag{3.8}$$

Replacing $\mathcal{L}_1$ from the above definition into the first component of Eq. (3.1) leads to the optimal boundary condition below:

$$\left[\boldsymbol{S}_1^{-1}\frac{\partial \boldsymbol{U}}{\partial t}\right]_1 + K(p - p_\infty) + \mathcal{L}_{t1} - \beta_t \overline{T}_1 = 0. \tag{3.9}$$

The above distinction between different transverse terms carries along modifications to the edges and coupling algorithm proposed by Lodato *et al.* (2008). These modifications are detailed in the next section.

4. Edges and corners coupling algorithm

The edges and corners coupling procedure (Lodato *et al.* 2008) is here adapted to the optimal formulation from Eq. (3.8). In order to derive the coupling relations for edges and corners, the Jacobians $\boldsymbol{A}^k$ are first conveniently decomposed such that the two different

contributions to the transverse terms are readily obtained. In fact, it is readily verified that if $\boldsymbol{A}^k$ is decomposed as

$$\boldsymbol{A}^k = \boldsymbol{A}^k_d + \boldsymbol{A}^k_t, \tag{4.1}$$

with $\boldsymbol{A}^k_d = u_k \boldsymbol{I}$, where $\boldsymbol{I}$ is the identity matrix, and $\boldsymbol{A}^k_t = \boldsymbol{A}^k - \boldsymbol{A}^k_d$, then the two different contributions to the transverse terms are obtained as [see Eq. (3.4)]

$$\boldsymbol{\mathcal{L}}_t = \boldsymbol{S}_1^{-1}\left(\boldsymbol{A}^2_d \frac{\partial \boldsymbol{U}}{\partial x_2} + \boldsymbol{A}^3_d \frac{\partial \boldsymbol{U}}{\partial x_3}\right), \tag{4.2}$$

$$-\overline{\boldsymbol{T}}^1 = \boldsymbol{S}_1^{-1}\left(\boldsymbol{A}^2_t \frac{\partial \boldsymbol{U}}{\partial x_2} + \boldsymbol{A}^3_t \frac{\partial \boldsymbol{U}}{\partial x_3}\right). \tag{4.3}$$

Let us consider the edge joining two subsonic outflows that are orthogonal to x_1 and x_2, and let us define the wave amplitude variations relevant to modes propagating along x_1 and x_2 as

$$\boldsymbol{\mathcal{L}} = \boldsymbol{S}_1^{-1}\boldsymbol{A}^1 \frac{\partial \boldsymbol{U}}{\partial x_1} \quad \text{and} \quad \boldsymbol{\mathcal{M}} = \boldsymbol{S}_2^{-1}\boldsymbol{A}^2 \frac{\partial \boldsymbol{U}}{\partial x_2}, \tag{4.4}$$

respectively. Premultiplying Eq. (2.4) by $\boldsymbol{S}_1^{-1}$ and $\boldsymbol{S}_2^{-1}$, after some manipulation involving the use of Eqs. (4.1) and (4.4), the following relations are obtained:

$$\boldsymbol{S}_1^{-1}\frac{\partial \boldsymbol{U}}{\partial t} + \boldsymbol{\mathcal{L}} + \boldsymbol{\mathcal{L}}_t + \underbrace{\boldsymbol{S}_1^{-1}\left(\boldsymbol{S}_2\boldsymbol{\mathcal{M}} - \boldsymbol{A}^2_d \frac{\partial \boldsymbol{U}}{\partial x_2} + \boldsymbol{A}^3_t \frac{\partial \boldsymbol{U}}{\partial x_3}\right)}_{-\overline{\boldsymbol{T}}^1} = \boldsymbol{0}, \tag{4.5}$$

$$\boldsymbol{S}_2^{-1}\frac{\partial \boldsymbol{U}}{\partial t} + \boldsymbol{\mathcal{M}} + \boldsymbol{\mathcal{M}}_t + \underbrace{\boldsymbol{S}_2^{-1}\left(\boldsymbol{S}_1\boldsymbol{\mathcal{L}} - \boldsymbol{A}^1_d \frac{\partial \boldsymbol{U}}{\partial x_1} + \boldsymbol{A}^3_t \frac{\partial \boldsymbol{U}}{\partial x_3}\right)}_{-\overline{\boldsymbol{T}}^2} = \boldsymbol{0}, \tag{4.6}$$

where

$$\boldsymbol{\mathcal{L}}_t = \boldsymbol{S}_1^{-1}\left(\boldsymbol{A}^2_d \frac{\partial \boldsymbol{U}}{\partial x_2} + \boldsymbol{A}^3_d \frac{\partial \boldsymbol{U}}{\partial x_3}\right), \tag{4.7}$$

$$\boldsymbol{\mathcal{M}}_t = \boldsymbol{S}_2^{-1}\left(\boldsymbol{A}^1_d \frac{\partial \boldsymbol{U}}{\partial x_1} + \boldsymbol{A}^3_d \frac{\partial \boldsymbol{U}}{\partial x_3}\right). \tag{4.8}$$

Assuming that the location of the boundaries is such that $\mathcal{L}_1$ and $\mathcal{M}_1$ are the unknown wave amplitude variations (see Lodato *et al.* 2008, Section 3.2.1.), the actual boundary conditions from Eq. (3.9) are

$$\left[\boldsymbol{S}_1^{-1}\frac{\partial \boldsymbol{U}}{\partial t}\right]_1 + K(p - p_\infty) + \mathcal{L}_{t1} - \beta_t \overline{T}^1_1 = 0, \tag{4.9}$$

$$\left[\boldsymbol{S}_2^{-1}\frac{\partial \boldsymbol{U}}{\partial t}\right]_1 + K(p - p_\infty) + \mathcal{M}_{t1} - \beta_t \overline{T}^2_1 = 0, \tag{4.10}$$

which, coupled with the first components of Eqs. (4.5) and (4.6), lead to the following system in the two unknown waves for the edge:

$$\mathcal{L}_1 = K(p - p_\infty) + (1 - \beta_t)\overline{T}^1_1, \tag{4.11}$$

$$\mathcal{M}_1 = K(p - p_\infty) + (1 - \beta_t)\overline{T}^2_1, \tag{4.12}$$

with

$$\overline{T}_1^1 = -\frac{1}{2}(\mathcal{M}_1 + \mathcal{M}_5 - \mathcal{M}_4) + \frac{u_2}{2}\left[\frac{1}{\rho a}\frac{\partial p}{\partial x_2} - \frac{\partial u_1}{\partial x_2}\right] - \frac{a}{2}\frac{\partial u_3}{\partial x_3}, \tag{4.13}$$

$$\overline{T}_1^2 = -\frac{1}{2}(\mathcal{L}_1 + \mathcal{L}_5 + \mathcal{L}_4) + \frac{u_1}{2}\left[\frac{1}{\rho a}\frac{\partial p}{\partial x_1} - \frac{\partial u_2}{\partial x_1}\right] - \frac{a}{2}\frac{\partial u_3}{\partial x_3}. \tag{4.14}$$

After grouping the unknown terms to the left, the linear system to be solved at the edge is

$$\begin{cases} \mathcal{L}_1 + \frac{1-\beta_t}{2}\mathcal{M}_1 = K(p - p_\infty) + (1-\beta_t)\widetilde{T}_1^1 \\ \frac{1-\beta_t}{2}\mathcal{L}_1 + \mathcal{M}_1 = K(p - p_\infty) + (1-\beta_t)\widetilde{T}_1^2 \end{cases}, \tag{4.15}$$

where $\widetilde{T}_1^1$ and $\widetilde{T}_1^2$ are now defined as

$$\widetilde{T}_1^1 = -\frac{1}{2}(\mathcal{M}_5 - \mathcal{M}_4) + \frac{u_2}{2}\left[\frac{1}{\rho a}\frac{\partial p}{\partial x_2} - \frac{\partial u_1}{\partial x_2}\right] - \frac{a}{2}\frac{\partial u_3}{\partial x_3}, \tag{4.16}$$

$$\widetilde{T}_1^2 = -\frac{1}{2}(\mathcal{L}_5 + \mathcal{L}_4) + \frac{u_1}{2}\left[\frac{1}{\rho a}\frac{\partial p}{\partial x_1} - \frac{\partial u_2}{\partial x_1}\right] - \frac{a}{2}\frac{\partial u_3}{\partial x_3}. \tag{4.17}$$

The corner coupling system can be easily obtained by analogy to what is done for the edge and is summarized below. After defining the wave amplitude variations relevant to modes propagating along x_3 as

$$\boldsymbol{\mathcal{N}} = \boldsymbol{S}_3^{-1}\boldsymbol{A}^3\frac{\partial \boldsymbol{U}}{\partial x_3}, \tag{4.18}$$

and supposing that the location of the boundaries is such that $\mathcal{L}_1$, $\mathcal{M}_1$ and $\mathcal{N}_1$ are the unknown wave amplitude variations, the modified transverse terms are

$$\overline{\boldsymbol{T}}^1 = -\boldsymbol{S}_1^{-1}\left(\boldsymbol{S}_2\boldsymbol{\mathcal{M}} + \boldsymbol{S}_3\boldsymbol{\mathcal{N}} - \boldsymbol{A}_d^2\frac{\partial \boldsymbol{U}}{\partial x_2} - \boldsymbol{A}_d^3\frac{\partial \boldsymbol{U}}{\partial x_3}\right), \tag{4.19}$$

$$\overline{\boldsymbol{T}}^2 = -\boldsymbol{S}_2^{-1}\left(\boldsymbol{S}_1\boldsymbol{\mathcal{L}} + \boldsymbol{S}_3\boldsymbol{\mathcal{N}} - \boldsymbol{A}_d^1\frac{\partial \boldsymbol{U}}{\partial x_1} - \boldsymbol{A}_d^3\frac{\partial \boldsymbol{U}}{\partial x_3}\right), \tag{4.20}$$

$$\overline{\boldsymbol{T}}^3 = -\boldsymbol{S}_3^{-1}\left(\boldsymbol{S}_1\boldsymbol{\mathcal{L}} + \boldsymbol{S}_2\boldsymbol{\mathcal{M}} - \boldsymbol{A}_d^1\frac{\partial \boldsymbol{U}}{\partial x_1} - \boldsymbol{A}_d^2\frac{\partial \boldsymbol{U}}{\partial x_2}\right), \tag{4.21}$$

and the linear system to be solved at the corner is

$$\begin{cases} \mathcal{L}_1 + \frac{1-\beta_t}{2}\mathcal{M}_1 + \frac{1-\beta_t}{2}\mathcal{N}_1 = K(p - p_\infty) + (1-\beta_t)\widetilde{T}_1^1 \\ \frac{1-\beta_t}{2}\mathcal{L}_1 + \mathcal{M}_1 + \frac{1-\beta_t}{2}\mathcal{N}_1 = K(p - p_\infty) + (1-\beta_t)\widetilde{T}_1^2 \\ \frac{1-\beta_t}{2}\mathcal{L}_1 + \frac{1-\beta_t}{2}\mathcal{M}_1 + \mathcal{N}_1 = K(p - p_\infty) + (1-\beta_t)\widetilde{T}_1^3 \end{cases}, \tag{4.22}$$

where $\widetilde{T}_1^1$, $\widetilde{T}_1^2$ and $\widetilde{T}_1^3$ are now defined as

$$\widetilde{T}_1^1 = -\frac{1}{2}(\mathcal{M}_5 + \mathcal{N}_5 - \mathcal{M}_4 + \mathcal{N}_3) + \sum_{k=2,3}\frac{u_k}{2}\left[\frac{1}{\rho a}\frac{\partial p}{\partial x_k} - \frac{\partial u_1}{\partial x_k}\right], \tag{4.23}$$

$$\widetilde{T}_1^2 = -\frac{1}{2}(\mathcal{L}_5 + \mathcal{N}_5 + \mathcal{L}_4 - \mathcal{N}_2) + \sum_{k=1,3}\frac{u_k}{2}\left[\frac{1}{\rho a}\frac{\partial p}{\partial x_k} - \frac{\partial u_2}{\partial x_k}\right], \tag{4.24}$$

$$\widetilde{T}_1^3 = -\frac{1}{2}(\mathcal{L}_5 + \mathcal{M}_5 - \mathcal{L}_3 + \mathcal{M}_2) + \sum_{k=1,2}\frac{u_k}{2}\left[\frac{1}{\rho a}\frac{\partial p}{\partial x_k} - \frac{\partial u_3}{\partial x_k}\right]. \tag{4.25}$$

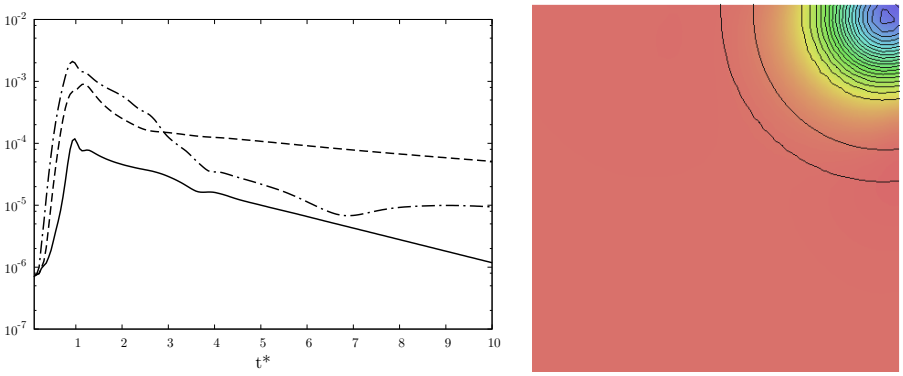

(a) $\mathcal{E}_{\mathrm{glb}}(p, t^*)$ (b)

FIGURE 1. Evolution of the global error in pressure as a function of the normalized time $t^* = t\,2u_\infty/L$ (a) and instantaneous pressure map with vorticity isolines (b): ——— , BC as per Eq. (3.9); – – – – – , 3D-NSCBC (Lodato *et al.* 2008); —·— , BC by Thompson (1990). The pressure map is represented over a quarter of the domain.

The above coupling algorithm is validated in the next section. In particular, the results obtained by using Eq. (3.9) in conjunction with the edge coupling algorithm are compared with the 3D-NSCBC formulation (Lodato *et al.* 2008) and the locally one-dimensional counterparts (Thompson 1990; Poinsot & Lele 1992).

5. Results and discussion

5.1. *Gaussian vortex test*

The present section addresses the specific problem of the transmission of vorticity through the corner of the computational domain. This is achieved by looking at the case of a convected Gaussian vortex convected at an angle of 45°. This is a very challenging test for boundary condition and it is generally advisable not to have complex flow structures crossing the edges and the corners of the grid.

The initial flow field at $t = 0$ was computed resorting to the following analytical solution for the inviscid vortex problem:

$$\frac{p(\boldsymbol{x},t)}{p_\infty} = \left[\frac{\rho(\boldsymbol{x},t)}{\rho_\infty}\right]^\gamma = \left[1 - C_v \exp\left(1 - \frac{\Delta x_1^2 + \Delta x_2^2}{R_v^2}\right)\right]^{\gamma/(\gamma-1)}, \tag{5.1}$$

$$u_1(x_1,x_2,t) = u_\infty \left[\frac{\sqrt{2}}{2} - \epsilon\frac{\Delta x_2}{R_v}\exp\left(\frac{1}{2} - \frac{\Delta x_1^2 + \Delta x_2^2}{2R_v^2}\right)\right], \tag{5.2}$$

$$u_2(x_1,x_2,t) = u_\infty \left[\frac{\sqrt{2}}{2} + \epsilon\frac{\Delta x_1}{R_v}\exp\left(\frac{1}{2} - \frac{\Delta x_1^2 + \Delta x_2^2}{2R_v^2}\right)\right], \tag{5.3}$$

with $C_v = 0.5\epsilon^2(\gamma-1)Ma_\infty^2$, $\Delta x_1 = x_1 - x_0 - u_\infty t\sqrt{2}/2$ and $\Delta x_2 = x_2 - y_0 - u_\infty t\sqrt{2}/2$. Ma_∞ was set at 0.42, whereas the vortex intensity and radius were specified setting $\epsilon = 0.08$ and $R_v = 0.1L$, respectively, where L is the side of the square computational domain (64×64 equally spaced cells extending from $-L/2$ to $L/2$ in both directions). The other reference quantities were $\rho_\infty = 1$, $p_\infty = 1$ and $\gamma = 1.4$.

The left and bottom boundaries were imposed as inviscid penalty terms (Carpenter

et al. 1994) computed from a fixed state coincident with the far field conditions. The top and right boundaries were treated using Eq. (3.9) and the coupling algorithm from Eqs. (4.5)–(4.6). The analytical solution from Eqs. (5.1)–(5.3) was used as a benchmark solution to quantify the performance of the outflow boundary condition by means of the global normalized error

$$\mathcal{E}_{\mathrm{glb}}(\phi,t)=\frac{\left[\sum_{i,j}\left(\phi_{i,j}(t)-\phi^{\mathrm{b}}_{i,j}(t)\right)^2\right]^{1/2}}{\left[\sum_{i,j}\left(\phi^{\mathrm{b}}_{i,j}(0)\right)^2\right]^{1/2}}, \tag{5.4}$$

where the superscript 'b' refers to the benchmark solution.

The global errors in density are plotted, as a function of the non-dimensional time $t^*=t\,2u_\infty/L$, in Figure 1. The errors obtained by using the boundary conditions from Thompson (1990) and Lodato *et al.* (2008) are also plotted for reference. An instantaneous map of pressure with vorticity contours is also shown when the vortex center reaches the corner of the domain. As expected in the cases where outgoing vorticity is involved, the optimal relaxation determines a significant reduction of the global error, which is about one order of magnitude lower than the one obtained with non-optimal relaxation, and more than one order of magnitude lower than that obtained using Thompson's BC.

5.2. *Pressure pulse test*

The computational domain was a square of side L, with 62×62 square control volumes and subsonic outflows according to Eq. (3.9) were applied on all the four faces. The corners of the computational domain were computed using Eqs. (4.5)–(4.6).

The pressure field was initialized with a circular pressure pulse of amplitude $\delta=0.001$:

$$p(r)=p_\infty\left[1+\delta\exp\left(-\frac{r^2}{2R_p^2}\right)\right], \tag{5.5}$$

where $r=\sqrt{x_1^2+x_2^2}$ is the distance from the center of the domain and $R_p=0.05L$ is the characteristic dimension of the pressure pulse. The temperature was set constant and equal to T_0 and the initial density distribution was computed according to the state equation $\rho(r)=p(r)/(\mathcal{R}T_0)$. The flow field was initialized at rest and then left to evolve.

In order to assess the performance of the formulation, a benchmark solution was computed on a computational domain four times bigger (i.e. $4L\times4L$ with 248×248 cells). The global error in pressure was then computed with Eq. (5.4) using the benchmark solution as a reference. The time history of the global error is shown in Figure 2 (note that the time is normalized using the sound speed, hence the pressure wave crosses the boundary at $t^*\sim1$). The errors obtained by using the boundary conditions from Thompson (1990); Poinsot & Lele (1992); Lodato *et al.* (2008) are also plotted for reference.

As expected, in the case of a purely acoustic wave, Eq. (3.9) and the 3D-NSCBC (Lodato *et al.* 2008) produce almost identical results (the curves are actually indistinguishable). In fact, the proposed optimal relaxation for transverse terms is expected to minimize, for the most part, acoustic reflection by outgoing vorticity (see Lodato *et al.* 2010). In agreement with Yoo *et al.* (2005), Yoo & Im (2007) and Lodato *et al.* (2008), the inclusion of transverse terms in the formulation of the incoming waves improves the results, giving about a three fold reduction in the error compared to formulations without transverse terms.

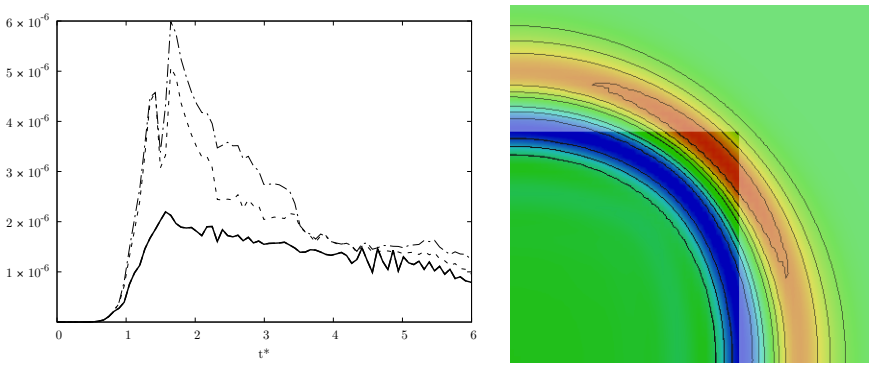

(a) $\mathcal{E}_{\mathrm{glb}}(p, t^*)$ (b)

FIGURE 2. Evolution of the global error in pressure as a function of the normalized time $t^* = t\,2a/L$ (a) and instantaneous pressure contours (b): ——— , BC as per Eq. (3.9); – – – – , 3D-NSCBC (Lodato *et al.* 2008); ····· , BC by Thompson (1990); —·— , BC by Poinsot & Lele (1992). Pressure contours are represented over a quarter of the test domain (lower left square) and part of the benchmark solution domain.

6. Concluding remarks

The role played by different transverse terms in the characteristic equations was carefully analyzed by Lodato *et al.* (2010, 2011) and a modified optimal formulation for the subsonic outflow boundary condition was proposed.

In particular, this optimal formulation included transverse effects in the computation of incoming modes at the boundary in a way that minimizes coupling between outgoing vorticity modes and incoming acoustic modes in a broad range of Mach numbers and base flow directions. In applications involving turbulent flows for which noise generation and propagation are the main concern, such a decoupling between vorticity and acoustic modes has the potential to significantly reduce spurious numerical noise generated when vortical structures cross the boundary.

When structured codes and cartesian grids are used, the above-mentioned modification to the characteristic subsonic outflow with transverse terms makes it necessary to reformulate the edges and corners coupling algorithm (Lodato *et al.* 2008) accordingly. The modified edges/corners procedure is detailed in the present work. Despite the significant changes in the mathematical development, the modifications that the new definition of the transverse terms carries along result in minor changes to the original edges and corners coupling procedure, thus allowing a relatively easy adaptation into existing implementations. Numerical tests involving a Gaussian vortex and an acoustic wave were provided in support of the proposed edges/corners algorithm.

Acknowledgments

The work was supported by NASA under the Subsonic Fixed Wing Program. The authors gratefully acknowledge Dr. J. Bodart for fruitful comments and for improving the quality of the final manuscript.

REFERENCES

BAYLISS, A. & TURKEL, E. 1982 Far field boundary conditions for compressible flows. *J. Comput. Phys.* **48** (2), 182–199.

Carpenter, M., Gottlieb, D. & Abarbanel, S. 1994 Time-stable boundary conditions for finite-difference schemes solving hyperbolic systems: Methodology and application to high-order compact schemes. *J. Comput. Phys.* **111**, 220–236.

Colonius, T. 2004 Modeling artificial boundary conditions for compressible flows. *Annu. Rev. Fluid Mech.* **36**, 315–345.

Giles, M. 1990 Nonreflecting boundary conditions for Euler equation calculations. *AIAA J.* **28** (12), 2050–2058.

Givoli, D. 1991 Non-reflecting boundary conditions. *J. Comput. Phys.* **94**, 1–29.

Givoli, D. 2004 High-order local non-reflecting boundary conditions: a review. *Wave Motion* **39** (4), 319–326.

Hedstrom, G. 1979 Nonreflecting boundary conditions for nonlinear hyperbolic systems. *J. Comput. Phys.* **30**, 222–237.

Hirsch, C. 1990 *Numerical Computation of Internal and External Flows*, , vol. 2. John Wiley & Sons Ltd.

Kreiss, H. 1970 Initial boundary value problems for hyperbolic systems. *Commun. Pure Appl. Math.* **23** (3), 277–298.

Lodato, G., Domingo, P. & Vervisch, L. 2008 Three-dimensional boundary conditions for direct and large-eddy simulation of compressible viscous flows. *J. Comput. Phys.* **227** (10), 5105–5143.

Lodato, G., Ham, F. & Pitsch, H. 2010 Subsonic characteristic outflow boundary conditions with transverse terms: a comparative study. In *Annual Research Briefs*, pp. 135–148. Center for Turbulence Research, Stanford University.

Lodato, G., Ham, F. & Pitsch, H. 2011 Optimal inclusion of transverse effects in non-reflecting characteristic boundary conditions. *AIAA J.* submitted.

Nicoud, F. 1999 Defining wave amplitude in characteristic boundary conditions. *J. Comput. Phys.* **149**, 418–422.

Poinsot, T. & Lele, S. 1992 Boundary conditions for direct simulations of compressible viscous flows. *J. Comput. Phys.* **101**, 104–129.

Roe, P. 1989 Remote boundary conditions for unsteady multidimensional aerodynamic computations. *Comput. Fluids* **17** (1), 221–231.

Rudy, D. & Strikwerda, J. 1980 A nonreflecting outflow boundary condition for subsonic Navier-Stokes calculations. *J. Comput. Phys.* **36**, 55–70.

Thompson, K. W. 1987 Time dependent boundary conditions for hyperbolic systems. *J. Comput. Phys.* **68**, 1–24.

Thompson, K. W. 1990 Time dependent boundary conditions for hyperbolic systems, II. *J. Comput. Phys.* **89**, 439–461.

Warming, R., Beam, R. & Hyett, B. 1975 Diagonalization and simultaneous symmetrization of the gas-dynamic matrices. *Math. Comput.* **29** (132), 1037–1045.

Yoo, C. & Im, H. 2007 Characteristic boundary conditions for simulations of compressible reacting flows with multi-dimensional, viscous and reaction effects. *Combust. Theor. Model.* **11** (2), 259–286.

Yoo, C., Wang, Y., Trouvé, A. & Im, H. 2005 Characteristic boundary conditions for direct simulations of turbulent counterflow flames. *Combust. Theor. Model.* **9** (4), 617–646.